Monthly Notices
of the
ROYAL ASTRONOMICAL SOCIETY

MNRAS **476,** 2591–2604 (2018)
Advance Access publication 2018 February 10

doi:10.1093/mnras/sty345

Galaxy pairs in the SDSS – XIII. The connection between enhanced star formation and molecular gas properties in galaxy mergers

Giulio Violino,[1]★ Sara L. Ellison,[2] Mark Sargent,[3] Kristen E. K. Coppin,[1] Jillian M. Scudder,[4] Trevor J. Mendel[5] and Amelie Saintonge[6]

[1]*Centre for Astrophysics Research, University of Hertfordshire, College Lane, Hatfield AL10 9AB, UK*
[2]*Department of Physics and Astronomy, University of Victoria, Finnerty Road, Victoria, British Columbia V8P 1A1, Canada*
[3]*Astronomy Centre, Department of Physics and Astronomy, University of Sussex, Brighton BN1 9QH, UK*
[4]*Department of Physics and Astronomy, Oberlin College, Oberlin, Ohio, OH 44074, USA*
[5]*Max-Planck-Institute fur Extraterrestrische Physik, Giessenbachstrasse, D-85748 Garching, Germany*
[6]*Department of Physics and Astronomy, University College London, Gower Street, London WC1E 6BT, UK*

Accepted 2018 January 26. Received 2018 January 23; in original form 2017 June 19

ABSTRACT

We investigate the connection between star formation and molecular gas properties in galaxy mergers at low redshift ($z \leq 0.06$). The study we present is based on IRAM 30-m CO(1–0) observations of 11 galaxies with a close companion selected from the Sloan Digital Sky Survey (SDSS). The pairs have mass ratios $\leq$4, projected separations $r_{\rm p} \leq 30$ kpc and velocity separations $\Delta V \leq 300\,{\rm km\,s^{-1}}$, and have been selected to exhibit enhanced specific star formation rates (sSFRs). We calculate molecular gas (H_2) masses, assigning to each galaxy a physically motivated conversion factor $\alpha_{\rm CO}$, and we derive molecular gas fractions and depletion times. We compare these quantities with those of isolated galaxies from the extended CO Legacy Data base for the *GALEX* Arecibo SDSS Survey sample (xCOLDGASS; Saintonge et al.) with gas quantities computed in an identical way. Ours is the first study which directly compares the gas properties of galaxy pairs and those of a control sample of normal galaxies with rigorous control procedures and for which SFR and H_2 masses have been estimated using the same method. We find that the galaxy pairs have shorter depletion times and an average molecular gas fraction enhancement of 0.4 dex compared to the mass matched control sample drawn from xCOLDGASS. However, the gas masses (and fractions) in galaxy pairs and their depletion times are consistent with those of non-mergers whose SFRs are similarly elevated. We conclude that both external interactions and internal processes may lead to molecular gas enhancement and decreased depletion times.

Key words: galaxies: evolution – galaxies: interactions – galaxies: ISM – radio lines: galaxies.

1 INTRODUCTION

Galaxy interactions represent a fundamental component of our current view of hierarchical galaxy evolution. Studies based on both observations and simulations have shown that galaxy collisions and mergers can dramatically affect the galaxies undergoing the interaction, by, e.g. triggering nuclear activity (e.g. Kennicutt 1984; Kennicutt et al. 1987; Ellison et al. 2011, 2013a; Silvermann et al. 2011; Satyapal et al. 2014), producing colour changes (e.g. Larson & Tinsley 1978; Darg et al. 2010; Patton et al. 2011), disrupting morphologies (e.g. Kaviraj et al. 2011; Patton et al. 2016; Lofthouse et al. 2017), and altering the metallicities (e.g. Rupke et al. 2010; Perez, Michel-Dansac & Tissera 2011; Scudder et al. 2012; Torrey et al. 2012). The most evident effect driven by galaxy encounters is probably the triggering of new episodes of star formation, which can occur both in the pre-merger regime between first pericentre and coalescence (e.g. Nikolic, Cullen & Alexander 2004; Ellison et al. 2008, 2013b; Patton et al. 2011; Scudder et al. 2012), and in the post-merger phase, where the two nuclei of the interacting galaxies have merged together (e.g. Kaviraj et al. 2012; Kaviraj 2014; Ellison et al. 2013a). The idea that galaxy mergers have a strong impact on the star formation activity is supported by studies of Ultra-Luminous InfraRed Galaxies (ULIRGs), i.e. galaxies with IR luminosities exceeding $10^{12}\,{\rm L_\odot}$ and characterized by star formation rates (SFRs) up to $\sim$1000 $\rm M_\odot\ yr^{-1}$ (e.g. Barnes & Hernquist 1991; Mihos & Hernquist 1994; Daddi et al. 2010; Scoville et al. 2015). Observations have revealed that the majority of ULIRGs

★ E-mail: g.violino@herts.ac.uk

reside in interacting systems (e.g. Sanders & Mirabel 1996; Veilleux, Kim & Sanders 2002; Kartaltepe et al. 2010, 2012; Haan et al. 2011). Nevertheless, ULIRGs are rare and extreme examples of highly star-forming galaxies. Most galaxy–galaxy interactions result in SFR increases of at most a factor of a few, as shown in both numerical simulations (e.g. Di Matteo et al. 2008) and observations of galaxy pairs and post-mergers (Ellison et al. 2008; Martig & Bournaud 2008; Jogee et al. 2009; Robaina et al. 2009; Scudder et al. 2012).

Theoretical work on galaxy encounters suggests that there are two main factors responsible for the enhancement of the star formation during a merger event. The first is an enrichment of the molecular gas reservoir available for fuelling star formation. This increase in the H_2 fraction can be explained by invoking an accelerated transition from atomic (HI) to molecular gas due to collision-induced external pressure (Kaneko et al. 2013b). Moster et al. (2011) present a physically motivated scenario for explaining this phenomenon from a set of cosmological hydrodynamical simulations of major mergers for which they include both a gas disc and a gas halo. This last component first drifts towards the centre of the galaxy and consequently cools down, causing a growth of the H_2 content. The second driver of enhanced star formation in mergers is an increase of the density of molecular gas, which induces a more efficient conversion of gas into stars. Indeed, numerical and hydrodynamical simulations predict that during the merger, gravitational torque decreases the angular momentum of gas which flows towards the galactic centre; the result is a rapid increase of the gas density which finally brings about a burst of nuclear star formation (Mihos & Hernquist 1996; Di Matteo et al. 2008; Renaud et al. 2014). Besides nuclear starbursts, interactions can also trigger highly efficient star formation across the whole galaxy through several episodes of gas fragmentation in dense clouds induced by gravitational torques, as was shown in high-resolution hydrodynamical simulations (Teyssier, Chapon & Bournaud 2010; Bournaud et al. 2011).

In order to test these theoretical predictions, numerous observational studies have investigated how the molecular gas content and the star formation activity are influenced by galaxy interactions, and how these vary across different phases of the merger. However, the majority of these have been hampered by several factors, including limited statistics [e.g. Braine et al. (2004) and Boquien et al. (2011) only studied single galaxy interactions], heterogeneous samples (often being a mix of pre-mergers and merger remnants, e.g. Braine et al. 1993; Casasola, Bettoni & Galletta 2004), and a lack of suitable control samples [e.g. Michiyama et al. (2016) used a comparison sample of only few sources with measurements of CO(3–2) from Tacconi et al. 2013].

Another complicating factor is the lack of a physically motivated conversion factor α_{CO} between the measured CO luminosity and molecular gas mass. In fact, a standard disc-like value has often been used for mergers ($\alpha_{CO} = 3.2$, e.g. Combes et al. 1994), which may not be appropriate, given that the interaction is capable of altering the ISM condition and morphology in the merging galaxies, which could result in a different relation between CO emission and H_2 content. In addition, more recent studies show that the conversion factor is not universal, varying from one source to another by up to a factor of $\sim 10^3$, depending on the gas surface density, metallicity, and stellar mass (e.g. Narayanan et al. 2012; Bolatto, Wolfire & Leroy 2013).

In this paper, we tackle these previous shortcomings by carefully selecting a sample of only galaxy pairs, adopting a physically motivated CO–H_2 conversion factor, and making use of the new extended *GALEX* Arecibo SDSS Survey (xCOLDGASS; Saintonge et al. 2017) to build a suitable comparison sample. We have carried out a systematic study of the molecular gas content (H_2), as traced by both the CO(1–0) and CO(2–1) using the IRAM 30-m, and the star formation activity of 11 galaxy pairs. Our main goal is to investigate the effects of galaxy interactions on the molecular gas component of the galaxies undergoing a merger, prior to the final coalescence stage (we study the molecular gas content of post-merger galaxies in a forthcoming paper: Sargent et al., in preparation). Specifically, we want to test whether the star formation enhancement exhibited by the galaxy pairs is related to either an enrichment of the gas content or to a decrease of the gas depletion time, or both.

This paper is organized as follows: in Section 2, we describe the sample selection of our galaxy pairs, while in Section 3 we describe the IRAM 30-m CO observations and data reduction. In Section 4, we present the analysis and our main results, which we discuss in Section 5. Finally, our conclusions are presented in Section 6 together with proposed future work to expand this study. Throughout this paper, we assume a Chabrier IMF and a flat ΛCDM cosmology with $H_0 = 69.6\,\mathrm{km\,s^{-1}\,Mpc^{-1}}$ and $\Omega_M = 0.286$ (Wright 2006).

2 SAMPLE SELECTION

In order to investigate the effect of galaxy interactions on the molecular gas content of mergers, we selected a sample of galaxies with a close spectroscopic companion. The parent sample is made up of more than 23 000 galaxy pairs (Ellison et al. 2008, 2010, 2011; Patton et al. 2011) from the Sloan Digital Sky Survey Data Release 7 (SDSS DR7; Abazajian et al. 2009), to which we applied the following criteria. First, the galaxy must have a close companion at a projected separation $r_p \leq 30\,\mathrm{kpc}$ and the velocity separation between the two galaxies must be $\Delta V \leq 300\,\mathrm{km\,s^{-1}}$; this latter condition maximizes our chance of selecting true interacting systems rather than objects lying close in the sky as a result of projection effects. Based on these criteria, the selected galaxies are most likely caught either prior to the first encounter, or soon after the first pericentre passage. Sources which reside at a more advanced phase in the merging event (i.e. after the second pericentre passage) usually exhibit smaller separations and a more pronounced disturbed morphology (e.g. Renaud et al. 2014). Next, to strictly select objects undergoing a major merger, we also imposed the constraint that the companion's stellar mass must be within a factor of 4 of its own. Since our target galaxy is not necessarily the primary (most massive) of the pair, the mass ratio of our sample ranges between 0.25 and 4 (see Table 1). To calculate stellar masses, we used the bulge+disc models from Mendel et al. (2014). Furthermore, the two galaxies which make up the pair must have a sufficiently large angular separation to avoid flux blending within the telescope beam. The IRAM 30-m beam full width at half-maximum (FWHM) is $\simeq$11 arcsec at 2 mm, therefore we imposed the angular separation of the pair to be at least $\geq$11 arcsec. In addition, a lower limit to the sSFR $\geq 3.9\,\mathrm{Gyr^{-1}}$ was also imposed, so that the galaxies of the sample have relatively high SFRs for their mass, as expected due to the triggering in mergers. In applying this cut, we relied on SFR estimates reported in the MPA/JHU catalogue (http://wwwmpa.mpa-garching.mpg.de/SDSS/DR7), and calculated following Brinchmann et al. (2004). Finally, in order to keep the exposure times to a reasonable value of $\leq$5 hr per source, a mass cut of $\log M_* \geq 9.5\,\mathrm{M_\odot}$ was imposed. The final sample which satisfies all the above criteria is made up of a total of 12 sources.

In Fig. 1, the SFR of our sample of pairs is compared with all star-forming galaxies, by computing an SFR offset (ΔSFR). This comparison method is analogous to our previous papers in this

Table 1. The main physical properties of the galaxy pairs sample. Stellar masses are calculated using the bulge+disc models from Mendel et al. (2014). r_p and ΔV represent the projected separation and the difference in velocity between the two members of the pair, respectively. The mass ratio is calculated between the stellar mass of the galaxy which we observed with IRAM and that of its companion. Note that this ratio varies between ∼0.25 and 4 as we only selected potential major mergers. SFRs are from the MPA/JHU catalogue and estimated through the method presented in Brinchmann et al. (2004). In the last column, aperture-corrected SFRs are reported, which represent the SFRs within the IRAM 30-m 22 arcsec beam and whose calculation is described in Section 4.2.

Source	SDSS DR7 objID	M_* (log $M_\odot$)	r_p (kpc)	ΔV (km s^{-1})	Mass ratio	Redshift	logSFR ($M_\odot$ yr^{-1})	logSFR^{aperture} ($M_\odot$ yr^{-1})
SDSSJ014845.47+134300.2	587724198282854532	9.71	26.59	127.0	2.57	0.045	0.34	0.25
SDSSJ080555.42+135959.0	587741489815028146	9.79	26.78	91.0	0.61	0.038	0.40	0.39
SDSSJ111633.85+284606.4	587741489835343908	9.47	16.66	27.0	0.72	0.024	−0.02	−0.11
SDSSJ112036.59+361234.4	587738616488853682	9.99	29.71	17.0	0.73	0.052	0.51	0.46
SDSSJ123935.85+163516.1	587742901789589569	9.72	19.55	118.0	3.90	0.026	0.16	0.09
SDSSJ125053.09+352404.9	587739304756641956	9.62	16.55	8.0	2.69	0.033	0.11	0.03
SDSSJ143154.09+215618.3	588023722049339476	10.58	20.55	13.0	3.70	0.044	1.69	1.68
SDSSJ143759.21+382154.4	588017603622142042	9.71	17.07	100.0	0.36	0.035	0.16	0.05
SDSSJ144819.69+090702.1	588017702411763744	9.54	22.04	68.0	3.13	0.029	0.19	0.03
SDSSJ145146.60+523510.6	587733603184607338	10.02	28.46	263.0	0.37	0.065	0.54	0.48
SDSSJ152819.60+530347.0	588011102640930946	10.16	27.77	145.0	0.30	0.053	0.62	0.60

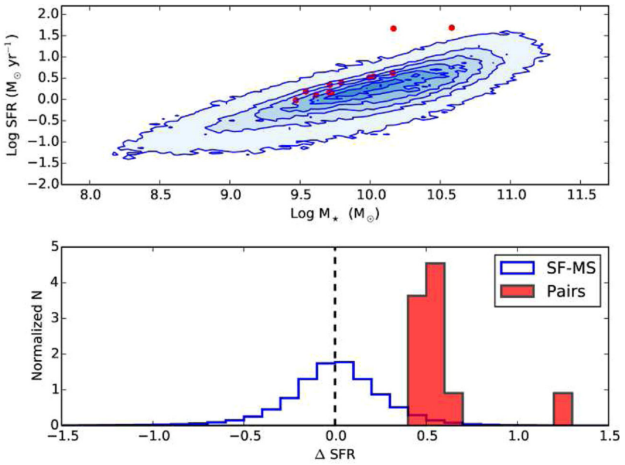

Figure 1. Top panel: Comparison between the main sequence of SDSS star-forming galaxies (blue contours, as classified by Kauffmann et al. 2003) and our sample of 11 galaxies in pairs (filled red circles). Stellar masses and total SFRs of both samples are taken from Mendel et al. (2014) and Brinchmann et al. (2004), respectively. Bottom panel: Distribution of the SFR offset of galaxies in pairs compared to the main sequence, which reveals enhanced star formation activity in our sample of 11 galaxy pairs. The procedure used to produce this plot is fully described in Ellison et al. (2016) and is summarized in Section 2.

series, employed to determine differences in SFR, colour, metallicity, HI content, and AGN fraction in mergers (Ellison et al. 2010, 2011, 2013a, 2015; Patton et al. 2011, 2013; Scudder et al. 2012; Satyapal et al. 2014). In brief, each galaxy in our pairs sample is matched in both redshift and stellar mass to a minimum of five control galaxies from the SDSS, with a nominal tolerance of 0.005 and 0.1 dex, respectively. These tolerances are allowed to grow by 0.005 and 0.1 dex, respectively, until the minimum required number of control sources is reached. The 'SFR offset' ΔSFR is defined as

$$\Delta\mathrm{SFR} = \log(\mathrm{SFR}^{\mathrm{tot}}, \mathrm{pair}) - \log(\mathrm{SFR}^{\mathrm{tot}}, \mathrm{control}), \quad (1)$$

where $\mathrm{SFR}^{\mathrm{tot}}$, pair and $\mathrm{SFR}^{\mathrm{tot}}$, control are the median total SFR of the galaxies in the pair and of the SDSS control sources, respectively. The mean SFR offset of our galaxy pairs is 0.5 dex, as illustrated in the bottom panel of Fig. 1.

3 OBSERVATIONS AND DATA REDUCTION

We observed 11/12 galaxies of our pairs sample with the IRAM 30-m telescope at Pico Veleta (Spain), between 2011 December 15 and 19, under generally good weather conditions ($0.04 \leq \tau_{225\,\mathrm{GHz}} \leq 0.25$, where $\tau_{225\,\mathrm{GHz}}$ represents the optical thickness). Our observing strategy aimed to achieve uniform $\geq 5\sigma$ CO(1–0) and CO(2–1) line-peak sensitivity across the whole sample, thus the integration time spent on each source varied between ∼18 and ∼300 min (see Table 2). The Eight Mixer Receiver (Carter et al. 2012) was used, which is characterized by two side bands of 8 GHz width each and two polarizations. Dual-band observations with the combination E0(3 mm)–E2(2 mm) were performed in order to observe the CO(1–0) and CO(2–1) lines simultaneously. Our galaxy mergers span the range $0.023 \leq z \leq 0.065$ with CO(1–0) and CO(2–1) redshifted between 108.210–112.675 and 216.417–225.345 GHz, respectively. We therefore set up the E2 receiver to cover the CO(2–1) line with three different tunings: 217.775, 221.667, and 224.283 GHz. The E0 receiver was correspondingly tuned to 108.889 GHz for the first E2 set-up and 111.503 for the other two. The Wideband Line Multiple Autocorrelator was used as the backend: it covers 4 GHz in each linear polarization for each band and gives a resolution of 2 MHz. As backup, the data were also recorded by the Fast Fourier Transform Spectrometers. Due to poor weather conditions, one source

Table 2. Details of the IRAM 30-m observations of local galaxy pairs. Total integration time, average atmospheric opacity at 225 GHz ($\tau_{225\,\mathrm{GHz}}$), and the number of scans per source are reported.

Source	Tot. Int. Time (min)	$\tau_{225\,\mathrm{GHz}}$	Number of scans
SDSSJ014845.47+134300.2	163.8	0.084	17
SDSSJ080555.42+135959.0	148.8	0.041	16
SDSSJ111633.85+284606.4	38.6	0.062	4
SDSSJ112036.59+361234.4	123.2	0.081	13
SDSSJ123935.85+163516.1	28.4	0.063	3
SDSSJ125053.09+352404.9	95.8	0.072	10
SDSSJ143154.09+215618.3	18.8	0.201	2
SDSSJ143759.21+382154.4	69.4	0.253	9
SDSSJ144819.69+090702.1	58.6	0.092	6
SDSSJ145146.60+523510.6	300.8	0.140	32
SDSSJ152819.60+530347.0	125.6	0.044	13

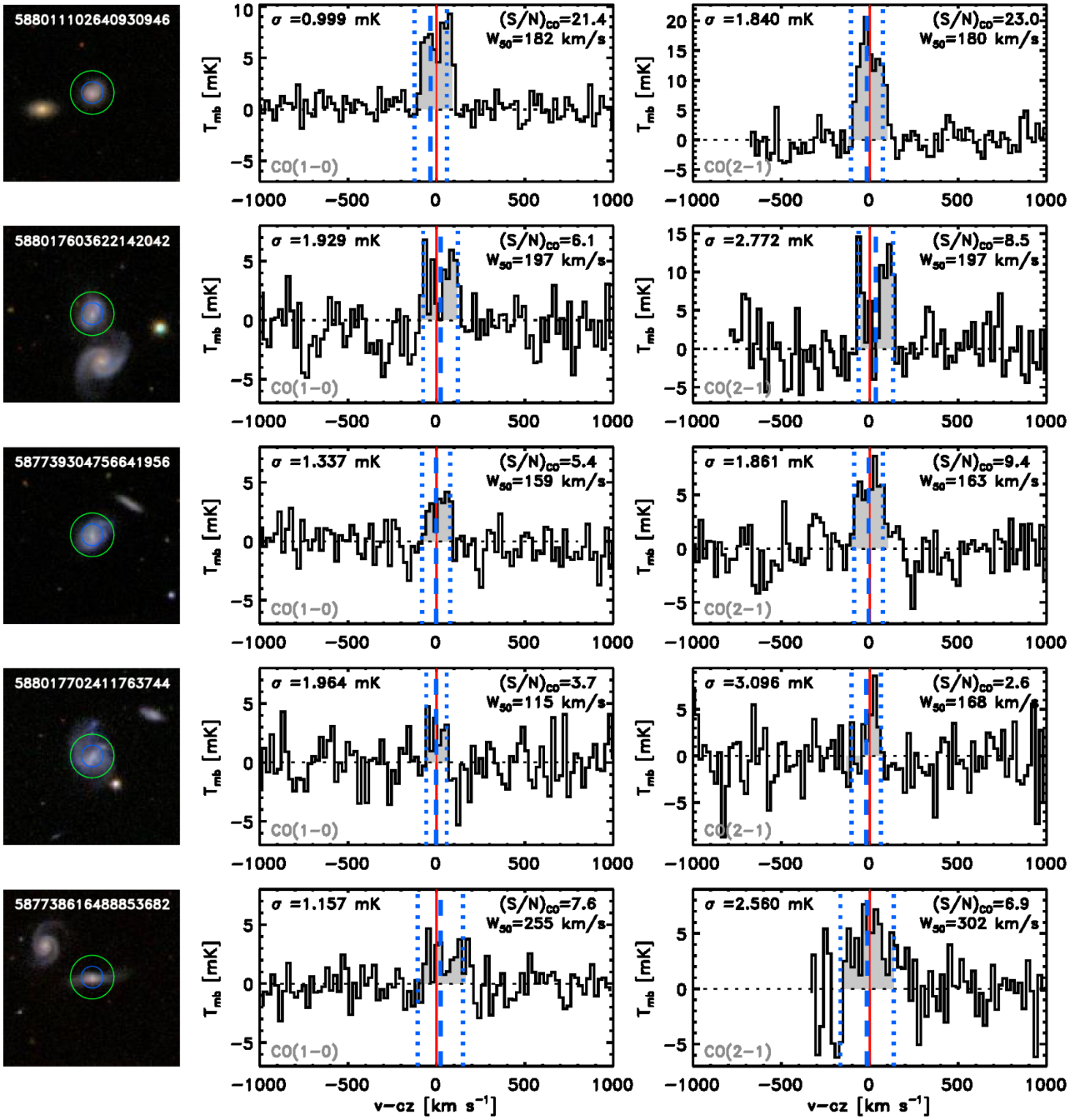

Figure 2. SDSS cutout images of the five galaxy pairs in our sample and their corresponding CO(1–0) (left) and CO(2–1) spectra (right). The green and blue circles in the images represent the FWHM size of the IRAM 30-m beam of 22 and 11 arcsec, respectively. In each spectrum, the red dashed line represents the systemic redshift of the source, as determined from the SDSS spectrum. The dashed blue line is the central velocity of the CO line, while the blue dotted line delimits $W50_{CO}$, i.e. the linewidth of the CO emission measured at half intensity.

could not be observed, therefore our study is based on a sample of 11 objects. In the left-hand panels of Fig. 2, we show the SDSS cutouts of the 11 interacting systems, with the galaxies we observed encircled in white with the beam size of the IRAM 30-m telescope at 3 mm.

The data reduction was carried out with the Continuum and Line Analysis Single-dish Software (http://www.iram.fr/IRAMFR/GILDAS); hereafter, we describe the standard reduction procedure for both CO (1–0) and CO(2–1) spectra, which is, for consistency, the same one adopted by Saintonge et al. (2011a) for the COLDGASS spectra. All the scans were visually examined, and those with severe baseline issues were rejected. The baseline of each scan was then fitted with a first-order polynomial and subtracted. All the scans belonging to the same observed galaxy are then combined together to generate an average spectrum which is later smoothed to a resolution of 20 km s^{-1}, yielding a 1σ channel rms of $\sim$1.5 mK. The total emission line flux I_{CO} is obtained by integrating the signal within a manually defined spectral window spanning the FWHM of the line.

The final spectra are shown in Figs 2 and 3, and the results of our reduction are presented in Table 3. The formal errors of the integrated line fluxes $I_{\rm CO}$ were calculated as

$$\sigma_I = \frac{\sigma_{\rm rms} W50_{\rm CO}}{(W50_{\rm CO}\Delta w^{-1})^{0.5}}, \quad (2)$$

where $\sigma_{\rm rms}$ is the rms noise per spectral channel of width $\Delta w_{\rm channel} = 21.57\,{\rm km\,s^{-1}}$ and $W50_{\rm CO}$ is the line width calculated as in Saintonge et al. (2011a).

4 ANALYSIS AND RESULTS

4.1 CO luminosities and molecular gas masses

To compute the molecular gas content of our targets, we calculate the CO line luminosities using the following equation (Solomon et al. 1997):

$$L'_{\rm CO} = 3.25 \times 10^7 I_{\rm CO} \nu_{\rm obs}^{-2} D_{\rm L^2} (1+z)^{-3}, \quad (3)$$

where $L'_{\rm CO}$ is the CO luminosity in K km s^{-1} pc^2, $I_{\rm CO}$ represents the line flux in units of Jy km s^{-1}, $\nu_{\rm obs}$ is the observed frequency of the line units of GHz, and $D_{\rm L}$ is the luminosity distance expressed in Mpc (see Table 3). In the following analysis, we only utilize the luminosity from the CO(1–0) transition, as this is the best tracer of the total molecular gas reservoir. The CO(2–1) transition, in fact, traces the gas which is in a slightly denser phase (e.g. Solomon & Vanden Bout 2005), and therefore provides a less accurate estimate of the total molecular gas reservoir. In addition, the IRAM beam size at 2 mm is characterized by an FWHM of 11 arcsec, and is therefore sensitive to the gas which only resides in the innermost part of the galaxy ($\leq$8 kpc). Excitation in the central region of the galaxies as traced by the $I_{\rm CO(2\text{-}1)}/I_{\rm CO(1\text{-}0)}$ ratio will be the subject of future work. The molecular hydrogen (H_2) masses within the IRAM 22 arcsec beam can be computed as $M^{\rm ap}_{\rm H_2} = L'_{\rm CO} \times \alpha_{\rm CO}$ (in the rest of the paper, we refer to $M^{\rm ap}_{\rm H_2}$ as simply $M_{\rm H_2}$). We compute CO-to-gas conversion factors $\alpha_{\rm CO}$ on a per-galaxy basis following the '2-Star Formation Mode (SFM)' framework of Sargent et al. (2014). Specifically, $\alpha_{\rm CO}$ values are calculated as

$$\alpha_{\rm CO} = (1 - f_{\rm SB}) \times \alpha_{\rm CO,MS} + f_{\rm SB} \times \alpha_{\rm CO,SB}, \quad (4)$$

where $f_{\rm SB}$ is the probability of a galaxy being in a starburst phase given its offset from the mean locus of the star-forming main sequence in the SFR–M_* plane (Sargent et al. 2012), while $\alpha_{\rm CO,\,MS}$ and $\alpha_{\rm CO,\,SB}$ are the CO-to-H_2 conversion factors expected in the 2-SFM formalism for a galaxy with the SFR and M_* values determined for a given galaxy in a pair. The main-sequence value $\alpha_{\rm CO,\,MS}$ varies with the galaxy metallicity following the Wolfire, Hollenbach & McKee (2010) prescription. $\alpha_{\rm CO,\,SB}$ deviates from the MS-$\alpha_{\rm CO}$ by an amount which depends on the intensity of the starburst [i.e. on the sSFR offset from the main sequence, see Sargent et al. (2014) for a full description of the underlying calculations]. For this sample, metallicities are taken from Tremonti et al. (2004).

In Table 4, we report the $f_{\rm SB}$ and $\alpha_{\rm CO}$ values estimated for each of our sources together with the H_2 masses. The conversion factor $\alpha_{\rm CO}$ varies between 0.97 and 7.60, with a median value of 2.29 $M_\odot$ (K km s^{-1} pc^2)$^{-1}$, i.e. about a factor of $\sim$2 lower than the canonical MW-conversion factor and reflecting the fact that galaxies in our sample are offset to high sSFRs.

Molecular gas masses span the range $8.5 \leq \log(M_*/{\rm M}_\odot) \leq 9.5$ with a mean value of $\log(M_*/{\rm M}_\odot) = 9.12$. Two factors contribute to the uncertainties on the H_2 masses: the error on the integrated line intensity $\sigma_{\rm I}$ ($\leq$ 2 per cent) and a flux calibration error which is $\sim$10 per cent for 3 mm observations (Saintonge et al. 2011a). The total average error is consequently $\sim$10 per cent. We do not include redshift uncertainties (which are negligible compared to the flux uncertainties), nor the systematic uncertainties involved in the calculation of $\alpha_{\rm CO}$ values (as these will affect conversion factors estimated for our control sample in exactly the same way).

4.2 Aperture SFRs

The FWHM of the IRAM 30-m telescope is 11 and 22 arcsec at 2 and 3 mm, respectively, corresponding to $\sim$8 and 16 kpc at the median redshift of our targets. For galaxies with extended gas distributions, CO flux from the outer part of the galaxy could thus potentially be missed by single-pointing observations (see Fig. 2). The most common approach to deal with this issue is to apply an aperture correction to the CO flux measurements. This is frequently done by utilizing resolved CO maps of similar sources (Regan et al. 2001; Kuno et al. 2007; Leroy et al. 2009) to estimate the amount of missed flux (Saintonge et al. 2011a; Bothwell et al. 2013), assuming a smooth gas profile which follows the distribution of stellar light. However, studies based on both isothermal simulations and spatially resolved maps show that during a galaxy encounter the distribution of molecular gas is less uniform, with CO emission located along tidal features, dust lanes or in extended discs (Shlosman, Frank & Begelman 1989; Konig et al. 2014; Ueda et al. 2014). For this reason, we adopt a slightly different approach to derive aperture corrections. Instead of applying a correction to the CO flux, to compute depletion times we have adjusted the SFRs in order to estimate the value of this quantity only within a 22 arcsec beam. For our sample, SDSS total SFRs are available from the MPA/JHU catalogue. These have been calculated either by modelling the emission lines with the Charlot & Longhetti (2001) models, or, if the galaxy hosts an AGN according to the Kauffmann et al. (2003) classification, by using the SFR–D4000 relation (Brinchmann et al. 2004). We thus calculate the fraction of the total r-band flux emitted within the 22 arcsec IRAM beam size and we multiply it by the total SFR from the MPA/JHU catalogue to obtain an aperture-converted SFR.

4.3 Comparison sample: xCOLDGASS

In order to robustly compare the molecular gas and the star-forming properties of our galaxy pairs with non-interacting galaxies, we require a carefully constructed comparison sample of 'normal' star-forming galaxies. The extended CO Legacy Data base for the *GALEX* Arecibo SDSS Survey (xCOLDGASS; Saintonge et al. 2017) represents the ideal sample for this purpose. COLDGASS (Saintonge et al. 2011a, 2012) is a legacy survey which studies the molecular gas of nearby late-type galaxies through IRAM 30-m CO(1–0) and CO(2–1) observations. It is comprised of 365 SDSS sources in the redshift range $0.0025 \leq z \leq 0.05$ with stellar masses $10 \leq \log(M_*/{\rm M}_\odot) \leq 11.5$. xCOLDGASS is an extension which also includes sources with masses down to $\log(M_*/{\rm M}_\odot) = 9$, bringing the total to 500 sources. Out of this extended sample, we only use galaxies with CO(1–0) detections and we additionally required a stellar mass measured by Mendel et al. (2014), which leaves 270 sources. Finally, in order to ensure that our control sample is made up of only 'isolated' star-forming galaxies, we excluded all those galaxies which have either a spectroscopic companion within 80 kpc and $\Delta V \leq 300\,{\rm km\,s^{-1}}$, or have a Galaxy Zoo merger vote fraction $\geq$0 (see Darg et al. 2010, for further details on this last criterion). The final xCOLDGASS subsample we take into consideration is thus formed of 186 galaxies. SDSS SFRs of xCOLDGASS

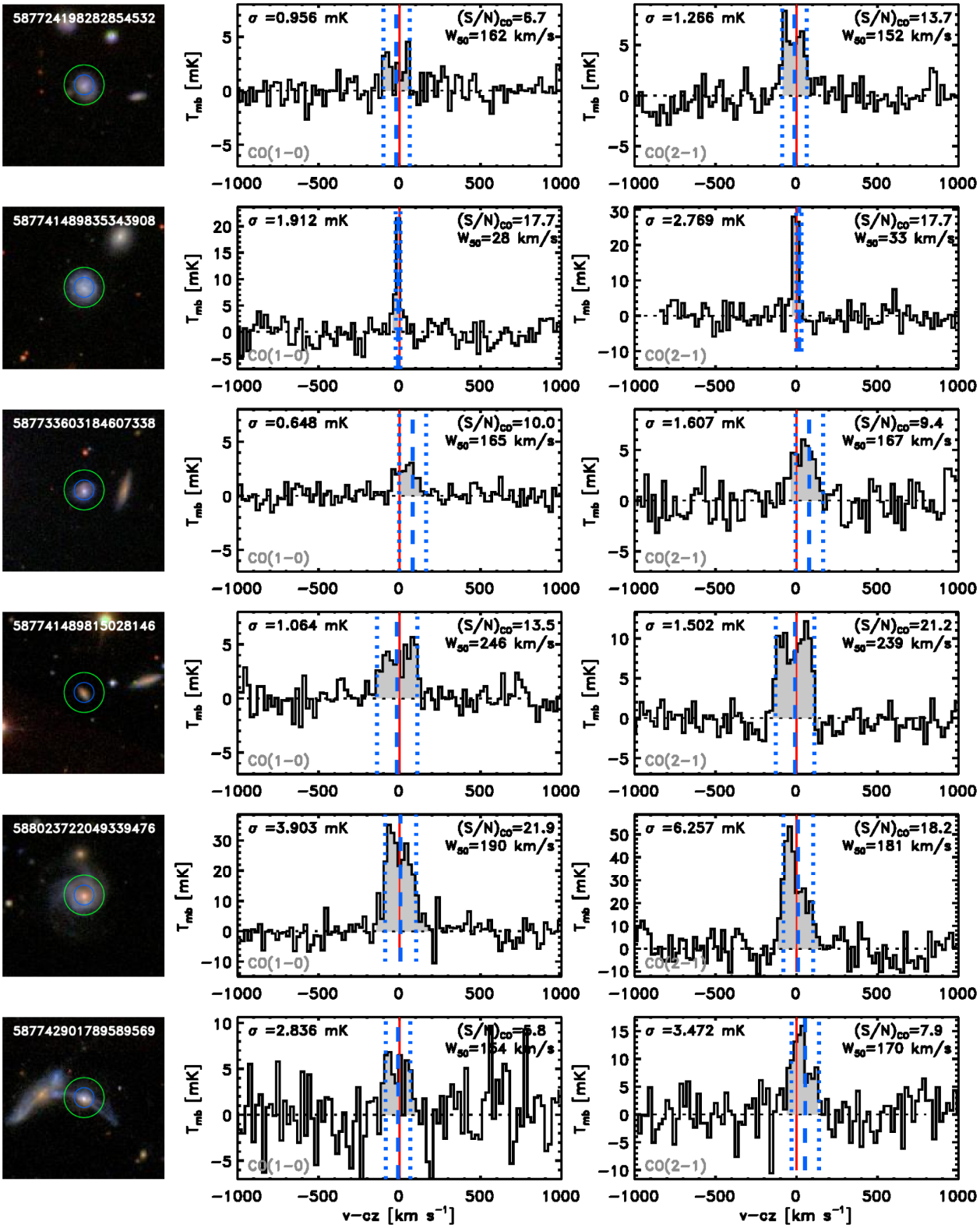

Figure 3. SDSS cutout images of the remaining six galaxy pairs in our sample and their corresponding CO(1–0) (left) and CO(2–1) spectra (right). Details as in Fig. 2.

galaxies have been aperture-corrected following the method described in Section 4.2. For consistency with our own measurements, H_2 masses are calculated by considering only the CO emission within the 22 arcsec IRAM beam, and by multiplying L'_{CO} by an α_{CO} conversion factor which varies for each source estimated using the method presented in Section 4.1. To summarize, the xCOLDGASS subsample we are employing in our analysis has stellar masses, SFRs, and molecular gas masses calculated with exactly the same

Table 3. Results from our CO (1–0) and (2–1) observations of our sample of 11 local mergers. CO emission line intensity (I_{CO}), width ($W50_{CO}$), and luminosity (L'_{CO}) are reported for each transition. The method to calculate these quantities is described in Section 3 and the corresponding spectra are shown in Figs 2 and 3.

Source	$I_{CO(1-0)}$ (Jy km s^{-1})	$W50_{CO(1-0)}$ (km s^{-1})	$L'_{CO(1-0)}$ (10^8 K km s^{-1} pc^2)	$I_{CO(2-1)}$ (Jy km s^{-1})	$W50_{CO(2-1)}$ (km s^{-1})	$L'_{CO(2-1)}$ (10^8 K km s^{-1} pc^2)
SDSSJ014845.47+134300.2	1.89 ± 0.05	164	1.79 ± 0.18	4.53 ± 0.05	153	1.05 ± 0.11
SDSSJ080555.42+135959.0	5.24 ± 0.06	259	3.49 ± 0.35	10.35 ± 0.07	239	1.76 ± 0.18
SDSSJ111633.85+284606.4	4.20 ± 0.04	29	1.06 ± 0.11	5.99 ± 0.05	33	0.38 ± 0.09
SDSSJ112036.59+361234.4	3.25 ± 0.07	270	4.07 ± 0.42	6.52 ± 0.11	209	2.06 ± 0.21
SDSSJ123935.85+163516.1	4.79 ± 0.13	154	1.48 ± 0.15	7.58 ± 0.13	165	0.59 ± 0.06
SDSSJ125053.09+352404.9	2.14 ± 0.05	166	1.06 ± 0.11	4.73 ± 0.11	162	0.59 ± 0.06
SDSSJ143154.09+215618.3	27.21 ± 0.21	200	24.89 ± 2.50	32.29 ± 0.26	190	7.34 ± 0.74
SDSSJ143759.21+382154.4	3.81 ± 0.10	208	2.20 ± 0.23	7.02 ± 0.12	199	1.01 ± 0.10
SDSSJ144819.69+090702.1	1.81 ± 0.08	115	0.72 ± 0.08	2.28 ± 0.124	18	0.23 ± 0.03
SDSSJ145146.60+523510.6	1.93 ± 0.03	178	3.85 ± 0.39	4.12 ± 0.06	167	2.06 ± 0.21
SDSSJ152819.60+530347.0	6.67 ± 0.05	183	8.81 ± 0.88	11.96 ± 0.07	180	3.96 ± 0.40

Table 4. Derived physical quantities of our sample of 11 local galaxies in pairs. The value f_{SB} is the probability of a pair galaxy to be in a starburst phase given its position in the SFR–M_* plane (see Section 4.1). The conversion factor α_{CO} has been calculated following Sargent et al. (2014) and described in Section 4.1; H_2 masses are derived from the CO(1–0) transitions. Molecular gas fractions are calculated as $f_{gas} = M_{H_2}/M_*$ and H_2 depletion times are $t_{dep} = M_{H_2}/SFR^{aperture}$. The average errors on gas masses, gas fractions, and depletion times are 10, 42, and 14 per cent, respectively (see the text for a description of their calculation).

Source	f_{SB}	α_{CO} [$M_\odot$ (K km s^{-1} pc^2)$^{-1}$]	log M_{H_2} [$M_\odot$]	f_{gas}	t_{dep} [Gyr] S
SDSSJ014845.47+134300.2	0.25	4.25	8.88	0.14	0.42
SDSSJ080555.42+135959.0	0.19	5.03	9.24	0.28	0.71
SDSSJ111633.85+284606.4	0.05	7.60	8.91	0.27	1.04
SDSSJ112036.59+361234.4	0.11	4.43	9.26	0.18	0.63
SDSSJ123935.85+163516.1	0.08	3.65	8.73	0.10	0.44
SDSSJ125053.09+352404.9	0.03	4.20	8.65	0.11	0.42
SDSSJ143154.09+215618.3	1.00	0.97	9.38	0.06	0.05
SDSSJ143759.21+382154.4	0.05	4.49	8.99	0.19	0.88
SDSSJ144819.69+090702.1	0.14	4.99	8.55	0.10	0.34
SDSSJ145146.60+523510.6	0.06	4.51	9.24	0.16	0.58
SDSSJ152819.60+530347.0	0.11	3.54	9.49	0.22	0.79

techniques as our 11 galaxy pairs, permitting a robust and like-for-like comparison.

4.4 Molecular gas masses

As a first step in our analysis, we compare the H_2 content in the 11 galaxy pairs with those of normal star-forming galaxies. Molecular gas fractions ($f_{gas} = M_{H_2}/M_*$) for our galaxy pairs are presented in Table 3. They vary from $0.06 \leq f_{gas} \leq 0.26$ with a median value of 0.16 ± 0.03. The average errors on the gas fractions are ∼42 per cent, taking into account both the errors on the H_2 masses and those on the stellar masses, which are on average ∼40 per cent (Mendel et al. 2014).

It is worth noting that the gas fractions obtained likely represent lower limits, since we are not including CO emission outside the IRAM 22 arcsec beam (which corresponds to a physical extent of ∼16 kpc). However, we also use this approach for the control sample, to ensure that the comparison analysis remains consistent. In Fig. 4, we plot the molecular gas fraction as a function of the stellar mass for both the 11 galaxies in pairs and the 186 sources from xCOLDGASS for a comparison. The blue dashed line is the best linear fit to the xCOLDGASS galaxies: as expected, the gas fraction decreases with increasing stellar mass, as found in numerous previous studies (e.g. Saintonge et al. 2011a; Bothwell et al. 2014). All the galaxies in pairs have higher gas content compared to normal galaxies, lying ∼0.4 dex above the general trend defined by the entire xCOLDGASS sample. To assess in a more statistical way the difference between the relative H_2 content of galaxy pairs with respect to the xCOLDGASS sample, we perform a Kolmogorov–Smirnov (KS) test, which can indicate whether or not two populations are drawn from the same underlying distribution of the gas fraction. The test returns a statistic of $D = 0.82$ with a p-value $= 4.125 \times 10^{-7}$, which corresponds to ≥ 99.99 per cent probability that the molecular gas fractions of our 11 interacting galaxies and those of normal galaxies belong to two intrinsically distinct distributions.

We now seek to compare each of our merging galaxies only with those sources from xCOLDGASS which exhibit similar underlying physical properties. We compute ΔM_{H_2}, which quantifies the discrepancy in the gas mass between interacting and isolated star-forming galaxies which lie in the same ranges of stellar mass, redshift, and local environment, quantified by the parameter δ_5. This quantity represents the local density, and is related to the distance of the galaxy neighbours (see Ellison et al. 2011, for a full description).

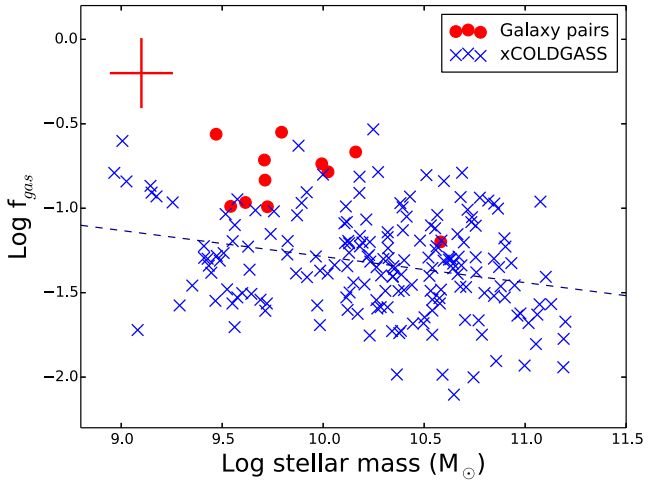

Figure 4. Molecular gas fraction $f_{\rm gas} = M_{\rm H_2}/M_*$ plotted as a function of the stellar mass M_* for our 11 galaxies in pairs (filled red circle) and xCOLDGASS sources (blue crosses). The red cross represents the average errors on gas fraction and stellar mass of our sample. Galaxy pairs display enhanced H_2 content, and lie on average ∼0.44 dex (∼1.3σ) above the dashed blue line which represents the best linear fit to xCOLDGASS galaxies.

The quantity $\Delta M_{\rm H_2}$ is analogous to ΔSFR presented in Section 2, and is defined as

$$\Delta M_{\rm H_2} = \log(M_{\rm H_2}, \text{pair}) - \log(M_{\rm H_2}, \text{control}), \quad (5)$$

where $\log(M_{\rm H_2}, \text{pair})$ and $\log(M_{\rm H_2}, \text{control})$ are the molecular gas masses of the galaxies in the pair and the mean gas fraction of the control sources, respectively. In carrying out this test, we adopted matching tolerances in all parameters of 0.005 dex and allowed two control sources per paired galaxy.

The top panel in Fig. 5 shows the distribution of $\Delta M_{\rm H_2}$ of the 11 galaxies in pairs compared to that of galaxies from xCOLDGASS. The median $\Delta M_{\rm H_2}$ of our sample is 0.34 dex, confirming the results from Fig. 4, and a KS test indicates that the $\Delta M_{\rm H_2}$ of our sample of galaxy pairs and that of the xCOLDGASS sample are drawn from two different distributions with a probability ≥ 99 per cent (p-value = $3.33\times\ 10^{-5}$). In order to test the effect of measurement errors in $M_{\rm H_2}$ on our calculation, for each galaxy of the pairs and xCOLDGASS samples we deviate the value of $M_{\rm H_2}$ by an amount sampled from within its Gaussian uncertainty, thus generating two artificial samples of galaxy pairs and isolated galaxies. We repeat this procedure 10 000 times, and for each iteration we perform a KS test between the $\Delta M_{\rm H_2}$ of the two artificial samples, and we register the number of times in which the two samples are statistically different at ≥3σ level (i.e. p-value ≤ 0.003). We find that the pairs and the xCOLDGASS sample belong to two different underlying distributions for all the 10 000 iterations.

Although our results indicate that galaxies in pairs have a higher molecular gas mass than non-interacting galaxies by about a factor of 2, we know that their SFRs are also enhanced (Fig. 1). In order to take into account the enhanced SFR of our paired galaxies, we repeat the analysis described above by adding an extra matching parameter, i.e. SFR, for which we apply the same tolerance of the other parameters (0.005 dex). In the bottom panel in Fig. 5, we show the new distribution of $\Delta M_{\rm H_2}$ of the 11 pairs sample and xCOLDGASS. The median $\Delta M_{\rm H_2}$ of the sample of galaxy pairs drops to 0.07 and a KS test between $\Delta M_{\rm H_2}$ of the pairs and 'normal' galaxies returns a p-value = 0.36, indicating that the two samples

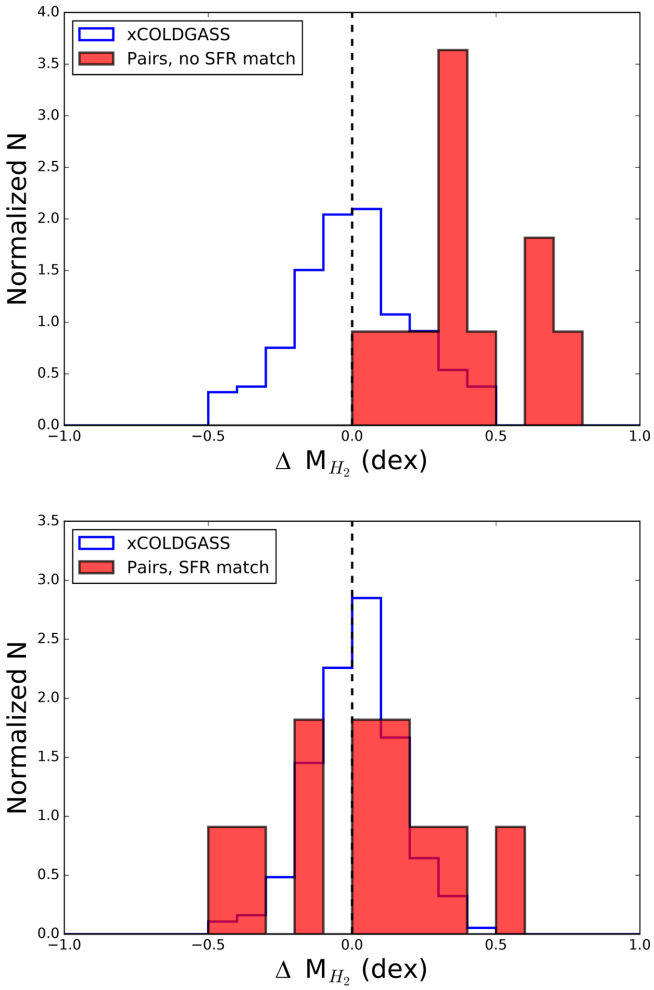

Figure 5. Distribution of molecular gas mass offset. Our sample of galaxy pairs is represented by the filled red histogram, whereas the xCOLDGASS sample distribution is plotted as a blue histogram. Top panel: $\Delta M_{\rm H_2}$ calculated employing as matching parameters stellar mass, redshift, and local density. Our pairs sample has a median $M_{\rm H_2}$ offset of 0.34 dex with respect to the control sample. Bottom panel: Same as above, with the addition of the SFR as matching parameters. The median offset $\Delta M_{\rm H_2}$ of the galaxy pairs is 0.07 dex.

are statistically indistinguishable. A bootstrap test shows that this result holds for the whole 10 000 iterations in which the $M_{\rm H_2}$ of galaxy pairs and xCOLDGASS galaxies are randomly resampled.

To summarize, although galaxy pairs show molecular gas mass enhancement relative to a stellar mass matched control, once we account for the relatively high sSFR of our sample, the difference in molecular gas content between galaxy pairs and xCOLDGASS sources seems to disappear. However, a caveat to this analysis is represented by the small number of xCOLDGASS sources capable of matching the pairs in all the parameters considered, particularly in SFR. In the future, a larger sample of control galaxies will be helpful in confirming this result.

4.5 Molecular gas depletion times

As demonstrated in Fig. 1, our galaxy pair sample is selected to exhibit enhanced (total) SFRs with respect to main-sequence galaxies. To investigate whether or not this enhanced SFR is entirely a result of the larger H_2 mass providing additional fuel for star formation,

we now directly study the molecular gas depletion time, defined as $t_{\rm dep} = M_{\rm H_2}/{\rm SFR}^{\rm aperture}$, which is (by definition) the inverse of the star formation efficiency (SFE). The depletion time represents the length of time which is necessary to consume the whole gas reservoir of a galaxy by converting it into new stars, assuming a constant rate of star formation and no replenishment of the gas reservoir nor any gas outflows.

For the pairs sample, we found the depletion time spans the range 0.05–1.04 Gyr with a median value of 0.57 ± 0.1 Gyr. The depletion time of the full xCOLDGASS galaxies varies between ∼0.14 and 110 Gyr with a median value of 1.7 ± 0.93 Gyr, approximately a factor of 2–3 longer than in the galaxy pairs. A KS test reveals $D = 0.62$ (p-value $= 2.2\times 10^{-4}$), which suggests that the depletion times of the 11 pairs and those of normal galaxies belong to two different distributions at a confidence level of $\gg 99.99$ per cent. For a more meaningful comparison of the gas consumption time-scales of interacting and normal galaxies, we again adopt the same technique used for the SFR and molecular gas masses comparison (i.e. we calculate a 'depletion time offset'). The procedure adopted here is identical to that described in Section 4.4, meaning that our 11 galaxies in pairs are first compared to two control sources from xCOLDGASS with matched redshift, stellar mass, and local density, and consequently the SFR is introduced as an extra matching parameter (we keep the same tolerance adopted before, i.e. 0.005). The quantity we consider here is the 'depletion time offset', $\Delta t_{\rm dep}$, which is therefore:

$$\Delta t_{\rm dep} = \log(t_{\rm dep}, {\rm pair}) - \log(t_{\rm dep}, {\rm control}). \quad (6)$$

The histograms in Fig. 6 show the $\Delta t_{\rm dep}$ distributions of our sample and that of xCOLDGASS. When the SFR is not included in the matching parameters, the median 'depletion time offset' of galaxies in pairs is −0.21 dex (top panel), indicating a depletion in the pairs that is 60 per cent shorter than in the control. A KS test produces a p-value $= 5.8\times 10^{-4}$, indicating that the difference between the samples is statistically significant. We then perform a bootstrap test analogous to that described above for the study of H_2 masses: in ∼87 per cent of the iterations (8761/10 000), the $\Delta t_{\rm dep}$ of galaxy pairs and control galaxies are drawn from a different distribution with a probability $\geq$ 99.97 per cent (which corresponds to a difference $\geq 3\sigma$, as previously done in the analysis of $\Delta M_{\rm H_2}$).

However, when the two control sources from xCOLDGASS are also matched in SFR, the median $\Delta t_{\rm dep}$ is 0.09 dex (the bottom panel of Fig. 5). A KS test applied to the 'depletion time offset' distributions drawn from the original samples of galaxy pairs and isolated galaxies from xCOLDGASS indicates that they are statistically indistinguishable (p-value $= 0.24$), and this is confirmed by the bootstrap test which shows that in none of the 10 000 iterations the null hypothesis that two artificial samples are drawn from the same underlying distributions can be rejected.

Thus, our sources appear to exhibit both higher gas masses and shorter depletion times when compared to normal galaxies compared with a mass matched sample of non-interacting galaxies drawn from xCOLDGASS. However, when additionally matched in SFR, these differences seem to disappear.

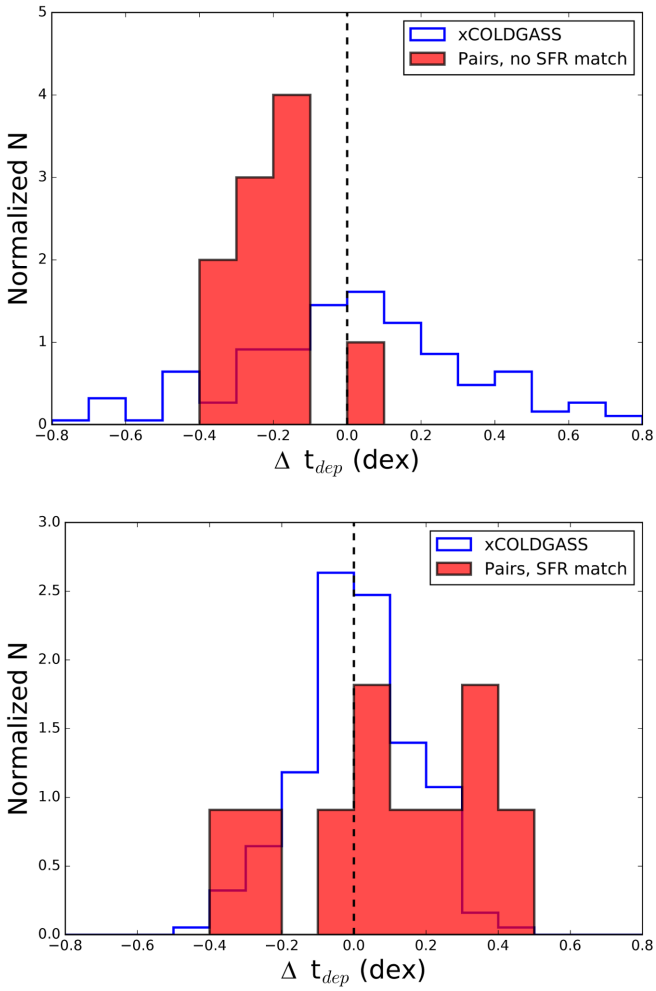

Figure 6. Molecular gas depletion time offset distribution of galaxy pairs (red filled histogram) and xCOLDGASS sources (blue empty histogram). Top panel: Comparison carried out using the following matching parameters: M_*, z, and δ_5. Our sample has a median offset from the matched control sample of −0.21 dex. Bottom panel: Same as above, with the inclusion of the SFR in the matching procedure; the median $\Delta t_{\rm dep}$ is 0.09.

5 DISCUSSION

The principal aim of this study is to investigate the connection between the gas properties and the star formation in galaxies at an early stage of a major merger. For this reason, we conducted a study of the molecular gas content and depletion time of a sample of 11 local galaxy pairs which display high sSFRs, as expected for galaxies with a close interacting companion. This is the first time (to our knowledge) that the gas properties of local galaxy pairs have been studied through a systematic comparison with that of normal galaxies, performing a homogeneous analysis for the merger and control samples. First, our method ensures that the main physical quantities we analysed, e.g. $M_{\rm H_2}$ and SFR, are calculated consistently between the sample of galaxy pairs and the comparison (control) sample to minimize any systematics. Secondly, we have used a physically motivated conversion factor to derive $M_{\rm H_2}$ from our CO observations. Again, this is done consistently for both the pairs and the control sample. Finally, we have constructed a subsample of control galaxies by carefully matching to stellar mass, SFR, redshift, and local density, so that we can robustly assess any offset between our pairs sample and the control sample.

5.1 Comparison with previous studies

We find that intensified star formation in galaxy pairs appears to be associated with an increase in the molecular gas content relative to the total mass by ∼ 0.4 dex (Figs 4 and 5). This result qualitatively

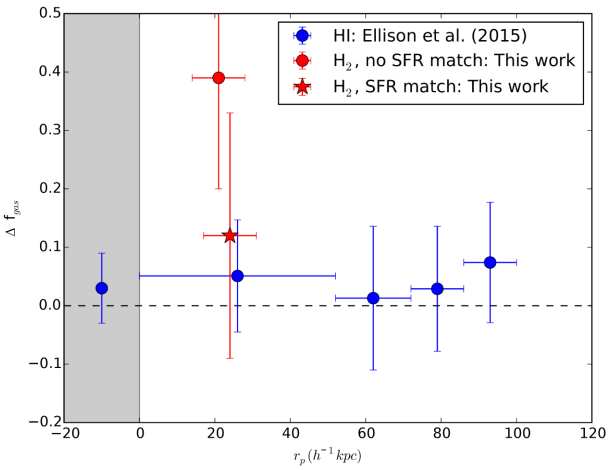

Figure 7. Distribution of the mean neutral gas fraction offset ($\Delta f_{\rm gas}$) as a function of projected separation. The blue circles are the pairs and post-merger galaxies from Ellison et al. (2015), whereas the red symbols represent the mean H_2 fraction offsets of the 11 galaxy pairs of this paper (red points are slightly offset on the *x*-axis for clarity). The method employed to calculate the H_2 fraction offset is identical to that described in Section 4.4.

confirms what has been seen previously, although the extent of the observed gas content enhancement varies amongst different studies. Combes et al. (1994) analysed a sample of 53 *IRAS*-detected galaxies in binary systems at redshift $z \sim 0$ and found that these sources are characterized by CO(1–0) luminosities which are, on average, one order of magnitude higher compared to local spirals, which consequently translates into higher molecular gas masses. One uncertainty in the Combes et al. (1994) study is the use of one conversion factor $\alpha_{\rm CO} = 3.68$ for the entire sample of galaxy pairs – a value reminiscent of the Milky Way and which could lead to an overestimation of the H_2 masses. Indeed, we find a variation of the $\alpha_{\rm CO}$ values in our sample with a typical value that deviates from the Galactic one by approximately a factor of 2. Similarly, Braine et al. (1993) observed low-redshift perturbed galaxies, which may reside in a more advanced phase of a merger than galaxy pairs, and argued that they contain more gas than normal disc galaxies by a factor of ∼2, with most of it residing in the centre of the galaxy. The same conclusion was reached by Ueda et al. (2014), who used ALMA resolved CO maps of post-mergers to show that their gas emission is mostly centrally concentrated. A slightly different result was reached by Kaneko et al. (2013a), who mapped the CO(1–0) emission in four early- and mid-stage mergers in the local Universe. They found that molecular gas in interacting galaxies is enhanced with respect to field galaxies ($f_{\rm gas}$ ∼0.2 dex higher in mergers), however, they found the concentration of molecular gas to be lower in the former.

One of the most popular scenarios invoked to explain the enhanced molecular gas content observed in galaxy mergers envisages the transition of galactic neutral gas (HI) to the molecular phase (Braine et al. 1993; Elmergreen 1993; Kaneko et al. 2013b). Interestingly, Ellison et al. (2015) carried out a similar analysis to that presented here, and showed no evidence of lower H I content (quantified by an H I fraction offset) in galaxies undergoing a merger, neither prior to the collision, nor in the post-merger phase. Following the method presented in Section 4 for gas mass offsets, we can equivalently compute gas fraction offsets for the pair galaxies relative to the xCOLDGASS control sample. In Fig. 7, we combine the gas fraction offsets that we determine for the molecular gas with the atomic gas fraction offsets from Ellison et al. (2015) in order to summarize changes in molecular and atomic gas fractions as a function of merger stage. As we previously found for molecular gas masses (Section 4.4), the H_2 gas fraction is elevated when compared to a mass matched sample, but consistent with the control when additionally matched in SFR. Sargent et al. (in preparation) have performed a similar analysis to the one presented here, but using a sample of post-merger galaxies, representing a later stage in the merger sequence than the pairs sample. Sargent et al. (in preparation) measure an enhanced molecular gas fraction of ∼ 0.6 dex relative to a mass and redshift matched control sample, qualitatively reproducing the enhanced molecular gas fraction found in our pairs sample. However, whereas the H_2 gas fraction enhancement in the pairs is no longer significant when the elevated SFRs are taken into account, the post-merger sample studied by Sargent et al. (in preparation) shows a persistent $\Delta f_{\rm gas} \sim 0.2$ even when the elevated SFRs are matched in the control sample.

Our next finding is that enhanced SFR in pairs is accompanied by a reduction of the time necessary to deplete the gas ($t_{\rm dep} \sim 0.6$ Gyr), which is about ∼0.5 dex shorter than in normal galaxies, represented by the whole xCOLDGASS sample. Combes et al. (1994) found that their sample of pairs exhibited depletion times up to ∼0.5 dex shorter than normal spirals. However, the depletion times in Combes et al. are likely underestimated because of the choice of a disc-like CO–H_2 conversion factor for their entire sample. Saintonge et al. (2012) analysed the depletion times of a subsample of COLDGASS sources classified as mergers based on their morphological features; this class of object has a mean depletion time of the order of 0.7 Gyr, a value which agrees with that found by our analysis. Goncalves et al. (2014) studied a sample of six Lyman break analogues, UV-selected star-forming galaxies in the local Universe. All their sources reside in galaxy pairs and their gas components constitute up to the 60 per cent of the total galaxy mass. However, despite lying along the sequence of normal star-forming galaxies in the Schmidt–Kennicutt plane, these galaxies will deplete their gas in less than ∼1 Gyr. It must be noted however that for these types of sources, the calculation of $M_{\rm H_2}$ can be particularly problematic, especially because of the uncertainties which affect the estimate of the CO–H_2 conversion factor. Indeed, these sources have both low metallicity and rather high SFRs, two characteristics which alter in opposite directions the derivation of $\alpha_{\rm CO}$ which can vary by a factor of ∼10 (Leroy et al. 2008; Papadopoulos et al. 2012). Casasola et al. (2004) instead found galaxy mergers to have the same molecular gas depletion times of normal galaxies ($t_{\rm dep}$ ∼1 Gyr). However, their sample was heterogeneous, including both post-mergers (i.e. galaxies exhibiting tidal features and disturbed structure) and galaxies in pairs. In addition, they also estimated molecular gas mass utilizing a single value of $\alpha_{\rm CO}$ for all their sources, regardless of the merger phase.

Importantly, we have also shown in Sections 4.4 and 4.5 that there are no differences in molecular gas content and depletion time between galaxy pairs and normal galaxies with matched physical properties (i.e. M_*, z, SFR, and δ_5). This however does not contradict previous results; instead, it indicates that an increase in the gas content and a reduction of the depletion time are also observable in normal galaxies, and *mergers are only one of the possible processes capable of inducing these effects*. For instance, stellar bar instabilities can cause an increase in the amount of dense gas and consequently drive enhanced star formation and a decrease of the gas consumption time-scale (e.g. Sheth et al. 2005; Wang et al. 2012).

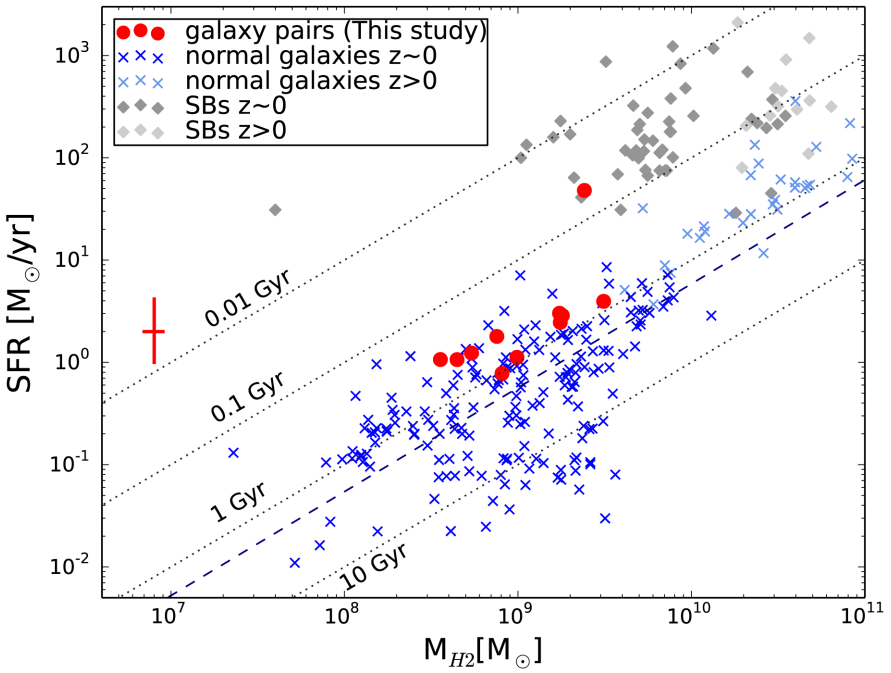

Figure 8. SFR plotted as a function of the molecular gas mass M_{H_2}. Our 11 galaxies in pairs are represented as red circles, while normal star-forming galaxies and starbursts are blue crosses and grey diamonds, respectively. For both literature samples, the dark symbols are local/low-redshift galaxies. The red cross reproduces the average error on M_{H_2} and SFR of our sample. For reference, we show lines of constant gas depletion time. The dashed blue line is the best fit to the normal galaxies; with galaxy pairs lying above this sequence (with an average offset $\leq 1\sigma$) as a result of their enhanced SFE.

5.2 The bimodality of the Schimidt–Kennicutt relation

It has been suggested that normal star-forming galaxies (discs and their high-z counterparts, BzK galaxies) and starbursts (local ULIRGs and SubMillimetre galaxies) form two different sequences in the SFR–M_{H_2} plane (Daddi et al. 2010; Genzel et al. 2010), with the latter having molecular gas depletion times up to ∼2 orders of magnitude shorter. However, more recently, Saintonge et al. (2011b) showed that the population of LIRGs can bridge the gap between the two sequences. In addition, Sargent et al. (2014) proposed that an apparent bimodality can arise because of poor sampling of intermediate sources, due to the fact that CO observing campaigns often favour either extreme star-forming objects or normal star-forming galaxies. We now wish to put our study in this context, and place our galaxy pairs in the integrated Schmidt–Kennicutt plane. To do this, we assemble a combination of normal galaxies and starbursts from the literature. We start with the compilation of Sargent et al. (2014), who selected 131 MS galaxies at redshift $z \leq 3$. To these, we add the subset of the xCOLDGASS sample described in 4.3 as well as local ULIRGs from the works of Solomon et al. (1997) and Combes et al. (2013). Moving to high-z, we include starburst galaxies from Bothwell et al. (2013), Rowlands et al. (2015), and Silvermann et al. (2015). We restrict these comparison samples by selecting only those sources which have observations of transitions not higher than CO(2–1), as this avoids uncertainties related to excitation correction when estimating the luminosity of the ground state CO(1–0) transition (to the contrary, Daddi et al. 2010 rely on previously observed sources which span a wide variety of CO transitions, from 1–0 up to 9–8). For sources with CO(2–1) measurements, we apply an excitation correction of 0.85 (Daddi et al. 2015). Our final comparison sample is made up of 277 sources in the redshift range 0.02–4, of which 216 are normal galaxies and 61 are starbursts. We also point out that in deriving the value of M_{H_2} for each of these sources, we adopt a conversion factor α_{CO} calculated with the same method used for our sample and described in Section 4.1.

In Fig. 8, we plot SFR as a function of H_2 mass for the composite literature sample together with our 11 galaxies in pairs. Determining the exact parametrization of the two sequences is beyond the scope of this paper, but we can examine the position of our sample relative to the two sequences. The 11 galaxy pairs lie systematically above the general relation defined by normal star-forming galaxies, as expected from the previous analysis, which showed that our sources have shorter depletion times when compared with the entire xCOLDGASS sample at fixed stellar mass. However, it can be also noted that a significant number of 'normal' galaxies exhibit similar SFRs to those of galaxy pairs (at fixed H_2 mass). This explains why, once that SFR is included as an extra matching parameter, the depletion times of galaxy pairs and control galaxies become comparable.

The locus of our galaxy pairs in the SFR–M_{H_2} plane is in agreement with that predicted by previous theoretical studies. For instance, Renaud et al. (2014) performed pc-scale hydrodynamical simulations of a galaxy merger, following the evolution in the Schmidt–Kennicutt plane of one of the interacting galaxies. According to their model, galaxies which are at the early stage of the merger, as in the case of our sources, display only a modest elevation above the sequence of disc galaxies. This is due to the fact that the gravitational interaction with the approaching companion is still weak and not capable of driving a drastic increase of the gas density. Consequently, as the merger proceeds, gas inflows gradually increase the surface density in the galactic nucleus, leading the source on the starburst sequence only between the second encounter and the final coalesce phase.

To summarize, our galaxy pairs appear to partially contribute to bridging the gap between the two sequences in the SFR–M_{H_2} plane. Sources which reside at a more advanced stage of the merger may

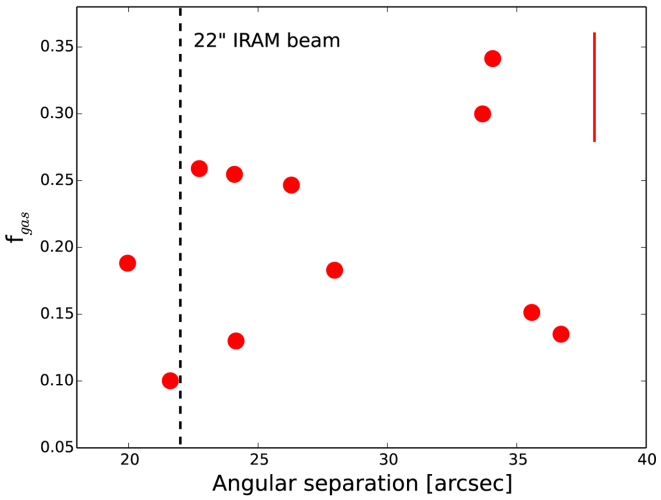

Figure 9. Molecular gas fraction versus angular separation between the two component galaxies comprising each pair in our sample. The red vertical bar represents the average error on gas fraction of our sample. The black dashed line indicates the FWHM of the IRAM 30-m beam at 3 mm. The majority of the sources lie above this limit, and together with the lack of correlation between the plotted quantities suggest that our CO measurements do not suffer from contamination from gas emission of the pair companion.

then begin to fill in the 'gap', as predicted by high-resolution hydrodynamical simulations (Powell et al. 2013; Renaud et al. 2014).

5.3 Caveats and limitations

We now consider any possible limitations and caveats to our results. First of all, for our CO flux measurements, we must consider the possibility of contamination from the CO emission of the companions, within the IRAM 30-m beam of 22 arcsec at 3 mm. In Fig. 9, we plot the molecular gas fraction as a function of the angular separation between the component galaxies in the pairs. No clear trend between these quantities is present, suggesting no systematic contamination from the companions. Furthermore, for the majority of our sources (9/11), the distance from the other member of the pair is well beyond the 22 arcsec (the size of the IRAM 30-m beam at 3 mm), and for the remaining two sources, the distance ($\sim$20 arcsec) is such that the potential contamination would only be marginal.

Secondly, amongst xCOLDGASS galaxies, we only select sources with CO detections, meaning that we are biased towards relatively gas-rich galaxies. However, we verified that the majority of the non-detected sources possess low SFR ($\log \mathrm{SFR} \leq -0.2$) and high stellar mass ($\log(M_*/\mathrm{M}_\odot) \geq 10$), and therefore cover a different parameter space than that of our galaxy pairs. As a consequence, their inclusion would not have an impact on our results. Similarly, the inclusion of CO-undetected sources in the SFR–$M_{\mathrm{H_2}}$ plane (Fig. 8) would alter the slope of the general relation defined by the xCOLDGASS sample, however our galaxy pairs would still lie well above it.

Another caveat which may affect our study is the calculation of the CO–$\mathrm{H_2}$ conversion factor. To date, the most recent models in the literature which attempt to provide a reliable value of α_{CO} are metallicity dependent (e.g. Wolfire et al. 2010; Narayanan et al. 2012, but see Bolatto, Wolfire & Leroy 2013 for a review on this topic). Similarly, the model we employed expresses the value of α_{CO} as a function of metallicity, SFR, and stellar mass. Importantly, the conversion factors have been estimated consistently between the sources of our sample and those of xCOLDGASS, therefore any systematics in our calculation of α_{CO} would affect the two samples in the same way.

Lastly, we want to stress that our results are not applicable to the entire population of merging galaxies, but only those galaxies which, through the interaction, gain a boost in their star formation activity. Both hydrodynamical simulations (Di Matteo et al. 2008; Powell et al. 2013) and observations (e.g. Saintonge et al. 2012) demonstrate that not all galaxy mergers are intrinsically associated with starbursts episodes.

6 CONCLUSIONS

In this paper, we present the results derived from our IRAM 30-m CO(1–0) and CO(2–1) observations of 11 SDSS-selected galaxies in pairs at $z \sim 0.03$. These sources represent the early stage of a major merger, and exhibit higher sSFR compared to main-sequence star-forming galaxies, as expected for galaxies undergoing an interaction. We study the molecular gas ($\mathrm{H_2}$) properties of these interacting systems through a comparison with a carefully selected control sample from xCOLDGASS (Saintonge et al. 2017). We find that:

(i) The molecular gas represents, on average, at least $\sim$16 per cent of the total stellar mass of our sources. Our sample of galaxy pairs exhibits molecular gas fractions $f_{\mathrm{gas}} = M_{\mathrm{H_2}}/M_*$ which are $\sim$0.4 dex higher than those of normal star-forming galaxies as sampled by xCOLDGASS galaxies. The enhanced (s)SFR seen in our galaxy pairs is therefore most likely driven by both a larger gas reservoir available for fuelling star formation, and by a higher efficiency in converting this gas into stars.

(ii) The average molecular gas consumption time-scale of our galaxy pairs is $\sim$0.6 Gyr. Compared with a mass matched control sample from xCOLDGASS, we find depletion times to be 0.2 dex shorter in pairs than in non-interacting galaxies. This decrease in the molecular gas depletion time reflects an enhancement of the efficiency in converting gas into stars; this is likely due to a faster transition of the molecular gas to its denser phase, driven by the gravitational interaction with a close companion.

(iii) If we additionally match the control sample in SFR, the molecular gas fractions and depletion times are consistent between the pairs and non-interacting galaxies. This suggests that even in normal galaxies, internal mechanisms (e.g. bar instabilities) can drive the same effect produced by galaxy interactions, such as enhancement of the molecular gas content, increase in SFR, and reduction of the molecular gas depletion time.

The results obtained in this paper can be used as a starting point for expanding the study of the gas properties in local galaxy mergers, and thus improve our view of the ISM conditions in this 'intermediate' class of star-forming galaxies. For this scope, additional observations are needed.

First of all, the companions of the 11 galaxies analysed in this study can be targeted in follow-up CO(1–0) and CO(2–1) observations, taking advantage of the successful observing strategy adopted here. In this way, it will be possible to study the effect of the merger on the molecular gas content of both the galaxies which make up a pair, gaining a complete view of this process. Secondly, observations of emission lines from higher CO transitions [e.g. CO(3–2) and CO(4–3)] of the 11 galaxy pairs of this sample would provide an insight into the physical conditions of the gas. In fact, through the study of the CO spectral line energy distribution, and a comparison with that of normal galaxies and starbursts (both at low and high redshift, e.g. Daddi et al. 2015), some crucial information such as

gas temperature and surface densities can be inferred (e.g. Lagos et al. 2012). Lastly, it has been suggested that the apparent bimodality in the integrated Schmidt–Kennicutt relation disappears once only the denser component of the molecular gas is considered (Gao et al. 2007 and reference therein). An expansion of our study to induce a probe of the dense phase (3×10^4 cm^{-2}) of the molecular gas (e.g. HCN) could shed some light on the apparently different global star formation laws that govern different types of sources.

ACKNOWLEDGEMENTS

GV acknowledges the University of Hertfordshire for a PhD studentship. KEKC acknowledges support from the UK Science and Technology Facilities Council (STFC; grant numbers ST/M001008/1, ST/J001333/1). JMS acknowledges support from the UK STFC Council (grant number ST/L000652/1).

This work is based on observations carried out with the IRAM 30-m telescope. IRAM is supported by INSU/CNRS (France), MPG (Germany), and IGN (Spain). The authors also acknowledge the IRAM staff for help provided during the observations and for data reduction. Funding for the SDSS and SDSS-II has been provided by the Alfred P. Sloan Foundation, the Participating Institutions, the National Science Foundation, the U.S. Department of Energy, the National Aeronautics and Space Administration, the Japanese Monbukagakusho, the Max Planck Society, and the Higher Education Funding Council for England. The SDSS web site is http://www.sdss.org/. The SDSS is managed by the Astrophysical Research Consortium for the Participating Institutions. The Participating Institutions are the American Museum of Natural History, Astrophysical Institute Potsdam, University of Basel, University of Cambridge, Case Western Reserve University, University of Chicago, Drexel University, Fermilab, the Institute for Advanced Study, the Japan Participation Group, Johns Hopkins University, the Joint Institute for Nuclear Astrophysics, the Kavli Institute for Particle Astrophysics and Cosmology, the Korean Scientist Group, the Chinese Academy of Sciences (LAMOST), Los Alamos National Laboratory, the Max-Planck-Institute for Astronomy (MPIA), the Max-Planck-Institute for Astrophysics (MPA), New Mexico State University, Ohio State University, University of Pittsburgh, University of Portsmouth, Princeton University, the United States Naval Observatory, and the University of Washington.

REFERENCES

Abazajian K. N. et al., 2009, ApJ, 182, 543
Barnes J. E., Hernquist L. E., 1991, ApJ, 370L, 65
Bolatto A. D., Wolfire M., Leroy A. K., 2013, ARA&A, 51, 207
Boquien M., Lisenfeld U., Duc P.-A., Braine J., Bournaud F., Brinks E., Charmandaris V., 2011, A&A, 533, 19
Bothwell M. S. et al., 2013, MNRAS, 429, 3047
Bothwell M. S. et al., 2014, MNRAS, 445, 2599
Bournaud F., Powell L. C., Chapon D., Teyssier R., 2011, IAUS, 271, 160
Braine J., Duc P. A., Lisenfeld U., Brinks E., Charmandaris V., Leon S., 2004, JAUS, 217, 518
Braine J., Combes F., 1993, A&A, 269, 7
Brinchmann J., Charlot S., White S. D. M., Tremonti C., Kauffmann G., Heckman T., Brinkmann J., 2004, MNRAS, 351, 1151
Carter M. et al., 2012, A&A, 538, 89
Casasola V., Bettoni D., Galletta G., 2004, A&A, 422, 941
Charlot S., Longhetti M., 2001, MNRAS, 323, 887
Combes F., Prugniel P., Rampazzo R., Sulentic J. W., 1994, A&A, 281, 725
Combes F., Garcia-Burillo S., Braine J., Schinnerer E., Walter F., Colina L., 2013, A&A, 550, A41
Daddi E. et al., 2010, ApJ, 714, L118
Daddi E. et al., 2015, A&A, 577, 46
Darg D. W. et al., 2010, MNRAS, 401, 1552
Di Matteo P., Bournaud F., Martig M., Combes F., Melchior A.-L., Semelin B., 2008, A&A, 492, 31
Ellison S. L., Patton D. R., Simard L., McConnachie W., 2008, AJ, 135, 1877
Ellison S. L., Prochaska J. X., Mendel J. T., 2010 MNRAS, 412, 448
Ellison S. L., Patton D. R., Mendel J. T., Scudder J. M., 2011, MNRAS, 418, 2043
Ellison S. L., Mendel J. T., Scudder J. M., Patton D. R., Palmer M. J. D., 2013a, MNRAS, 430, 3128
Ellison S. L., Mendel J. T., Patton D. R., Scudder J. M., 2013b, MNRAS, 435, 3627
Ellison S. L., Fertig D., Rosenberg J. L., Nair P., Simard L., Torrey P., Patton D. R., 2015, MNRAS, 448, 221
Ellison S. L., Teimoorinia H., Rosario D. J., Mendel J. T., 2016, MNRAS, 455, 370
Elmergreen B. G., 1993, ApJ, 411, 170
Gao Y., Carilli C. L., Solomon P. M., Vanden Bout P. A., 2007, ApJ, 660, 93
Genzel R. et al., 2010, MNRAS, 407, 2091
Goncalves T. S., 2014, MNRAS, 442, 1429
Haan S. et al., 2011, AJ, 141, 100
Jogee S. et al., 2009, ApJ, 697, 1971
Kaneko H., 2013a, PASJ, 65, 20
Kaneko H., 2013b, ASPC, 477, 83
Kartaltepe J. S. et al., 2010, ApJ, 721, 98
Kartaltepe J. S. et al., 2012, ApJ, 757, 23
Kauffmann G., White S. D. M., Heckman T. M., Ménard B., Brinchmann J., Charlot S., Tremonti C., Brinkmann J., 2003, MNRAS, 353, 713
Kaviraj S., Tan K.-M., Ellis R. S., Silk J., 2011, MNRAS, 411, 2148
Kaviraj S., 2014, MNRAS, 440, 2944
Kaviraj S. et al., 2012, MNRAS, 423, 49
Kennicutt R. C., 1984, ApJ, 279, 5
Kennicutt R. C., Roettiger K. A., Keel W. C., van der Hulst J. M., Hummel E., 1987, NASCP, 2466, 401
König S., Aalto S., Lindroos L., Muller S., Gallagher J. S., Beswick R. J., Petitpas G., Jütte E., 2014, A&A, 569, A6
Kuno N. et al., 2007, PASJ, 59, 117
Lagos C. del P., Bayet E., Baugh C. M., Lacey C. G., Bell T. A., Fanidakis N., Geach J. E., 2012, MNRAS, 426, 1242
Larson R. B., Tinsley B. M., 1978, ApJ, 219, 46L
Leroy A. K., Walter F., Brinks E., Bigiel F., de Blok W. J. G., Madore B., Thornley M. D., 2008, AJ, 136, 2782
Leroy A. K. et al., 2009, AJ, 137, 4670
Lofthouse E. K., Kaviraj S., Conselice C. J., Mortlock A., Hartley W., 2017, MNRAS, 465, 2895
Martig M., Bournaud F., 2008, MNRAS, 385, L38
Mendel J. T., Simard L., Palmer M., Ellison S. L., Patton D. R., 2014, ApJS, 210, 3
Michiyama T. et al., 2016, PASJ, 90
Mihos J. C., Hernquist L. E., 1994, ApJ, 431, 9
Mihos J. C., Hernquist L. E., 1996, ApJ, 464, 641
Moster B. P., Macciò A. V., Somerville R. S., Naab T., Cox T. J., 2011, MNRAS, 415, 3750
Narayanan D., Krumholz M., Ostriker E., Hernquist L., 2012, MNRAS, 421, 3127
Nikolic B., Cullen H., Alexander P., 2004, MNRAS, 355, 874
Papadopoulos P. P., van der Werf P., Xilouris E., Isaak K. G., Gao Y., 2012, ApJ, 751 10
Patton D. R., Ellison S. L., Simard L., McConnachie A. W., Mendel J. T., 2011, MNRAS, 412, 591
Patton D. R., Torrey P., Ellison S. L., Mendel J. T., Scudder J. M., 2013, MNRAS, 433, 59
Patton D. R., Qamar F. D., Ellison S. L., Bluck A. F. L., Simard L., Mendel J. T., Moreno J., Torrey P., 2016, MNRAS, 461, 2589
Perez J., Michel-Dansac L., Tissera P. B., 2011, MNRAS, 417, 580

Powell L. C., Bournaud F., Chapon D., Teyssier R., 2013, MNRAS, 434, 1028
Regan M. W., Thornley M. D., Helfer T. T., Sheth K., Wong T., Vogel S. N., Blitz L., Bock D. C.-J., 2001, ApJ, 561, 218
Renaud F., Bournaud F., Kraljic K., Duc P-A., 2014, MNRAS, 442, 33
Robaina A. R. et al., 2009, ApJ, 704, 324
Rowlands K., Wild V., Nesvadba N., Sibthorpe B., Mortier A., Lehnert M., da Cunha E., 2015, MNRAS, 448, 258
Rupke D. S. N., Kewley L. J., Chien L.-H., 2010, ApJ, 723, 1255
Saintonge A. et al., 2011a, MNRAS, 415, 32
Saintonge A. et al., 2011b, MNRAS, 415, 61
Saintonge A. et al., 2012, MNRAS, 415, 32
Saintonge A. et al., 2017, ApJS, 233, 22
Sanders D. B., Mirabel I. F., 1996, ARA&A, 34, 749
Sargent M., Bethermin M., Daddi E., Elbaz D., 2012, ApJ, 747, 31
Sargent M. T. et al., 2014, ApJ, 793, 19
Satyapal S., Ellison S. L., McAlpine W., Hickox R. C., Patton D. R., Mendel J. T., 2014, MNRAS, 441, 1297
Scoville N. A. et al., 2015, ApJ, 800, 70
Scudder J. M., Ellison S. L., Torrey P., Patton D. R., Mendel T. J., 2012, MNRAS, 426, 549
Sheth K., Vogel S. N., Regan M. W., Thornley M. D., Teuben P. J., 2005, ApJ, 632, 217
Shlosman I., Frank J., Begelman M. C., 1989, Nature, 338, 45
Silverman J. D. et al., 2011, ApJ, 743, 2
Silverman J. D. et al., 2015, ApJ, 812, 23
Solomon P. M., Vanden Bout P. A., 2005, ARA&A, 43, 677
Solomon S., Downes D., Radford S. J. E., Barret J. W., 1997, ApJ, 478, 144
Tacconi L. J. et al., 2013, ApJ, 768, 74
Teyssier R., Chapon D., Bournaud F., 2010, ApJ, 720, 149
Torrey P., Cox T. J., Kewley L., Hernquist L., 2012, ApJ, 746, 108
Tremonti C. A. et al., 2004, ApJ, 613, 898
Ueda J. et al., 2014, ApJS, 214, 1
Veilleux S., Kim D.-C., Sanders D. B., 2002, ApJ, 143, 315
Wang Y., Zhao H., Mao S., Rich R. M., 2012, MNRAS, 427, 1429
Wolfire M. G., Hollenbach D., McKee C. F., 2010, ApJ, 716, 1191
Wright E. L., 2006, PASP, 118, 1711

This paper has been typeset from a TEX/LATEX file prepared by the author.